https://doi.org/10.18321/ectj862

Influence of Various Parameters on the SCS Ni/NiO Nanostructures and their Mechanism of Formation

O. Thoda[1,2], G. Xanthopoulou[1,3]*, G. Vekinis[1], A. Chroneos[2]

[1]Institute of Nanoscience and Nanotechnology, NCSR "Demokritos", AgiaParaskeviAttikis, 15310, Greece
[2]Faculty of Engineering, Environment and Computing, Coventry University, Priory Street, CV1 5FB, Coventry, UK
[3]Samara State Aerospace University, Moskovskoye Hwy, 34, Samara, 443086,Russia

Article info

Received:
19 November 2018

Received in revised form:
16 January 2019

Accepted:
6 March 2019

Abstract

Solution combustion synthesis (SCS) is an efficient approach to deliver materials with desirable properties directly in the nanoscale. Nevertheless, it is a very sensitive method and there are many parameters that influence the final materials' properties and microstructure. In this work, four parameters that severely affect the combustion mechanism of formation for the final products, and as a result their final properties, are studied. These are the concentration of nitrates, the concentration of fuel in direct and slow heating and the time in furnace after the SCS is completed. It has been concluded that all these parameters affect the SCS process in a complicated way and an attempt has been made to explain the underlying mechanisms and processes that shape the final nanostructures. Finally, some of the as-synthesized Ni/NiO nanopowders were employed as catalysts and their activity was tested in the liquid-phase hydrogenation of maleic acid.

1. Introduction

A combination of combustion synthesis and reactive solution methods leads to solution combustion synthesis (SCS) [1]. SCS, which was firstly proposed by Patil et al. [2], is being used widely to prepare oxide materials for numerous applications. In the case of SCS, the exothermicity of the redox chemical reaction is employed to manufacture advantageous materials, as it is an easy, cheap and versatile approach [3].

It typically involves a cascade of self-sustained redox reactions in a homogeneous water solution of reactants. The most common reagents are metal nitrates (oxidizers) and various fuels, which can be classified according to their chemical structure; that is the type of reactive groups bonded to the hydrocarbon chain [4]. The reaction between fuel and oxygen-containing species, which are formed during the nitrites decomposition, provides high-temperature rapid interaction. In most cases, a precursor aqueous solution of reactants is preheated to a temperature range between 150–200 °C, the water evaporates, the remaining reacting solution dries up and its temperatures further increases. Within a few seconds up to few minutes, it ignites and a quick exothermic reaction takes place and results in powder forms directly in the nanoscale [5–7].

The unique characteristic of the SCS-derived materials are originated to certain features of this method. The initial reaction takes place in the aqueous phase permitting the reactants to mix on a molecular level, thus facilitating the formation of narrow and consistent nanosized products [8]. Furthermore, the high reaction temperature (T_c) results in high purity and crystallinity of the synthesized products. This feature is very important as it helps in skipping the additional step of high-temperature product calcinations that in many cases follows the conventional approaches, to achieve the desired phase composition. Finally, the short reaction time and the emission of many gaseous products during SCS inhibit the particles' growth benefiting the synthesis of nanocrystalline powders with high specific surface area [9–10].

There are many parameters that influence the composition, microstructure and properties of the

*Corresponding author.
E-mail: g.xanthopoulou@inn.demokritos.gr

final SCS products. The concentration of reactants, the diluent's nature and the pH level of the precursor solution are crucial parameters. Furthermore, the nature, the type of the fuel and the fuel to oxidizer ratio are also important factors for the synthesis of desired materials [11–16].

In the present study, a systematic assessment of various parameters that influence the final products' properties as well as the mechanism that results in that effect is reported.

2. Methodology

A temperature profile analyzer was employed in order to study the temperature evolution during the combustion process. The pyrex beaker containing the initial SCS mixture is placed in the preheated furnace at 500 °C. There are three 100 μm type K (chromel/alumel) thermocouples connected to a multiple input thermometer for temperature measurement, mounted in the lid and they are placed in and above the solution. A PICO TC-08 was used to record the temperature signals at a rate of 0.5 ms.

For in-situ observation of the combustion process and study of the dynamics of phase formation in the reaction front of the combustion, wave time-resolved (dynamic) X-ray diffraction (DXRD) was used. Diffracted X-rays from the sample are recorded in the horizontal plane by using a 1-dimensional position-sensitive detector which can receive data over a range of 2θ of 30° to 75°.

Crystal structure was examined by X-ray diffraction analysis on a Siemens Spellman DF3 spectrometer with Cu-Kα radiation. XRD patterns were recorded in an angle range (2θ) between 5 and 100 degrees and with step 0.03°/sec. For semi-quantitative XRD analysis, 10%wt. KCl was added in all samples as an internal standard, in order to calculate the relative quantity of each phase. The hkl of nickel peak is 111, of nickel oxide 101 and of potassium chloride 100.

A GAPP V-Sorb 2800 porosimetry analyser was employed for the BET specific surface area and pore size distribution measurements. Nitrogen and helium were used as carrier gases. The examined samples were pretreated before analysis, where they were subjected into degasing under vacuum ($3 \cdot 10^{-4}$ Torr) in two gradual temperature stages (80 and 150 °C) for 45 min each.

An FEI CM 20 analytical High Resolution Transmission Electron Microscope (TEM) equipped with an EDAX Electron Dispersive X-ray Spectroscopy (EDS) system and a GIF200 Gatanenergy filter was utilized for TEM studies.

The activity of the SCS catalysts synthesised was studied in liquid-phase hydrogenation of unsaturated hydrocarbons(H/C).The installation consists of a shaker-reactor in a water bath kept stable the selected temperature for reaction. One gram of catalyst is added in the catalytic reactor with 30 ml of distilled water. After this, the unsaturated hydrocarbon is added (0.26 g) in calculated quantity for reaction with 50 ml of hydrogen at atmospheric pressure. Both catalyst saturation with hydrogen and hydrogenation are carried out under continuous mechanical stirring (360–380 rpm). Measurements of the amount of reacted hydrogen are taken every minute at atmospheric pressure. To check reproducibility, each hydrogenation test was repeated at least three times. The reproducibility was found to be within ±5% [25–26].

3. Results and discussion

3.1. Influence of the nickel nitrate concentration

The precursor SCS mixture consisted of mixtures of nickel nitrate hexahydrate [$Ni(NO_3)_2 \cdot 6H_2O$] as oxidizer and glycine as fuel. Four samples were studied with different quantities (3, 6, 9, 12 g) of the oxidizer, 50%wt (of the oxidizer)glycine and 75 ml of distilled water. All the prepared solutions were heated on a hot plate with mild magnetic stirring until 70 °C. After that pre-heating, each solution was placed in a pre-heated furnace at 500 °C in air atmosphere. After the end of the combustion synthesis, the sample was removed from the furnace and left to cool down at room temperature.

The phases that were synthesized during solution combustion synthesis were detected using X-Ray diffraction analysis and the received patterns are shown in Fig. 1 below.

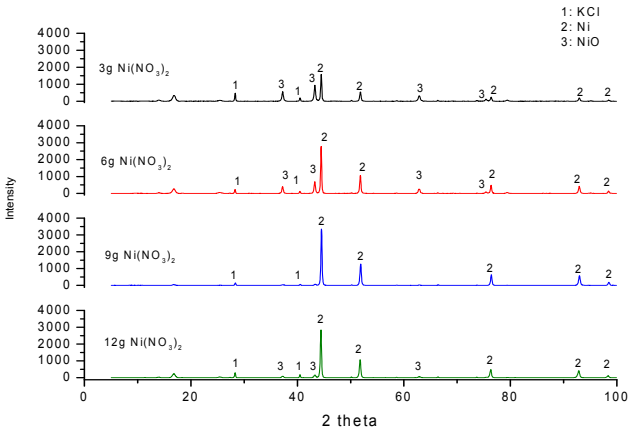

Fig. 1. Development of crystal structure of SCS catalysts on the basis of initial composition of $Ni(NO_3)_2$, 50% glycine and 75 ml distilled H_2O.

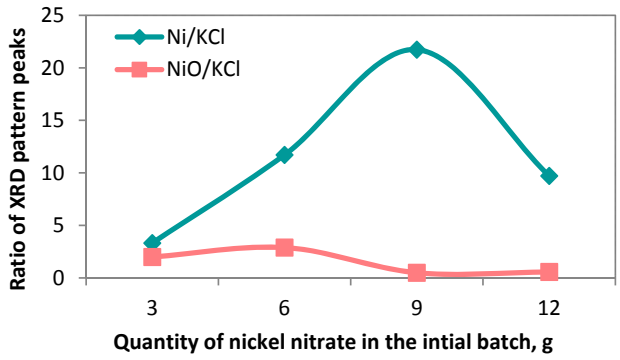

Fig. 2. Semi-quantitative analysis of Ni and NiO phases in the resulting materials.

The two phases produced by SCS were metallic nickel and nickel oxide (NiO), as determined by XRD analysis. The relative phase composition of Ni and NiO, as determined by the comparative X-Ray diffraction analysis, as a function of nickel nitrate quantity in the precursor mixture are presented in Fig. 2.

Figure 2 shows that the concentration of metallic nickel in the resulting product increases when the quantity of nickel nitrate increases up to 9 g in the initial mixture. Interestingly, with further increase of nickel nitrate to 12 g the concentration of nickel is reduced in the final material. The increase of the oxidizer quantity affects only the generated heat from the combustion, thus the cooling time is prolonged. On the other hand, there is a specific time for the formation of nickel as well as for its oxidation. Thus, the maximum can be attributed to the initial increase of time for nickel formation, while after exceeding 9 g, there is enough time for nickel oxidation as well. It is of high importance to have high nickel content in the final products, as they will be employed as catalysts toward liquid-phase hydrogenation and nickel is the active phase for this catalytic reaction.

3.2. Influence of the fuel quantity

Four samples were synthesized by changing the quantity of glycine in the precursor solution. Each solution contained 9.34 g nickel nitrate, 75 ml distilled water and glycine in four different amounts (50, 75, 100 and 125 wt% of nickel nitrate). All the prepared solutions were heated in a borosilicate glass on a hot plate with mild magnetic stirring until 70 °C. The beaker was then placed in a pre-heated furnace at 500 °C and after the end of combustion the beaker was removed from the furnace and left to cool in room temperature.

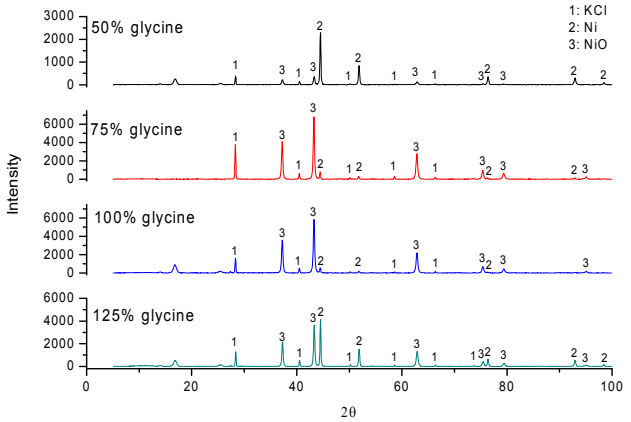

Fig. 3. Development of the crystal structure of an SCS material on the basis of nickel nitrate hexahydrate with various glycine concentrations and 100 ml water as diluent.

The production of the compounds in the SCS–derived products is presented in the XRD patterns demonstrated on Fig. 3.

As it is illustrated on Fig. 3, cubic nickel and nickel oxide are the products of the SCS in various concentrations. The products were examined using TEM analysis and the results are demonstrated on Fig. 4 below.

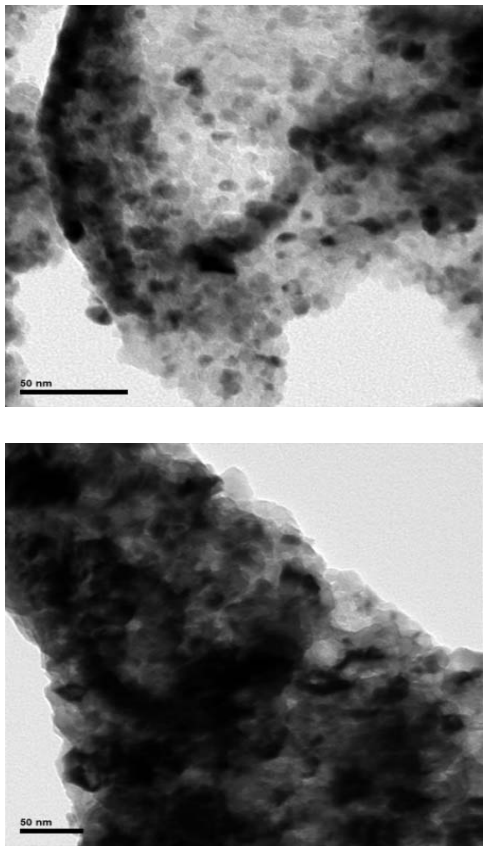

Fig. 4. TEM images of the sample prepared with 50% glycine in the initial solution.

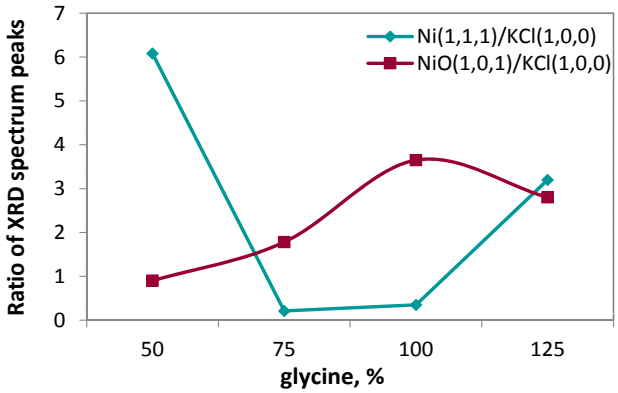

Fig. 5. Semi-quantitative SCS final composition dependence from glycine concentration in SCS mixture [$Ni(NO_3)_2 \cdot 6H_2O$, glycine, 100 ml H_2O].

TEM bright field images of areas consist of 5–12 nm crystallites (a) and of 15–50 nm crystallites (b). They demonstrate that the as-synthesized crystallites and by extension, the SCS product is directly synthesized at nanoscale.

The dependence of the relative phase composition of Ni and NiO on the quantity of glycine added in the precursor SCS solution is presented in Fig. 5 where the variation between Ni/KCl and NiO/KCl are shown together for comparison.

According to Fig. 5 above, the maximum nickel content in the SCS products occurs at the position of the minimum nickel oxide content when the amount of glycine employed in the initial solution is 50%. It appears that at this point, there is an optimum ratio between ammonia and nitric acid that react and produce hydrogen, creating a reduction atmosphere for the synthesis of nickel from nickel oxide. Conversely, as the glycine concentration increases up to 100% the nickel oxide content in the final product is maximized with a minimum of nickel. Initially, the increase of carbon concentration in the mixture leads to an increase of the reaction temperature, making the oxidation of the reduced nickel quicker. With further increase of glycine to 100%, the soot oxidation reaction is favoured on the expense of the nickel oxide reduction. Thus, the carbon originated from glycine is employed to the soot oxidation reaction yielding carbon monoxide and carbon dioxide. Additionally, the ammonia produced by glycine is in much excess for the reaction with nitric acid and as a result their non-stoichiometric reaction produces a relatively small amount of hydrogen. The combination of the small amount of produced hydrogen and the consumption of carbon in the oxidation reaction resulted in reduction of nickel content in the SCS product. On the other hand, when the glycine quantity reaches 125%, the combustion temperature rises and the carbon concentration is so high that both the nickel oxidation and the reduction of nickel oxide take place, resulting in the enhancement of the nickel concentration in the final product. Notably, in this case, carbon is the major element that reduces nickel oxide for the production of nickel, and not hydrogen as it was in the case of 50% glycine.

Brunauer–Emmett–Teller (BET) analysis was employed to perform measurements that provided information about the samples' pore shape, pore volume and specific surface area. The results are presented in the figures that follow.

Five types of hysteresis loops are categorized and associated with different pore shapes according to De Boer [17]. Type A hysteresis related to cylindrical pores; type B corresponds to slit-shape pores; types C and D hysteresises are correlated to wedge-shape pores and type E hysteresis is attributed to bottle neck pores. Adsorption-desorption curves obtained by the BET method are shown in Fig. 6 for all four synthesized materials.

The samples with 75 and 100% glycine that provided the (b) and (c) curves adsorbed the most nitrogen at the highest pressure, while the other two adsorbed the least nitrogen, indicating little microporosity. Moreover, all tested samples provided a hysteresis loop but the samples with 50 and 125% of glycine exhibited a distinct hysteresis loop, suggesting that the evaporation from the pores is a completely different process from the condensation in the pores, which indicates the occurrence of capillary condensation within mesopores [18]. Regarding the shape of the hysteresis loops, the adsorption/desorption isotherms of samples with 50 and 125% glycine (a and d isotherms correspondingly) correspond to type B, suggesting the existence of large number of cylindrical and slit-shape pores with all open sides. On the other hand, the type of loop in samples with 75 and 100% glycine (b and c isotherms accordingly) are type C indicating that the pores have a predominately wedge shape. The pore shape affects the adsorption/desorption processes during catalysis influencing the catalysts' activity.

The dependence of the measured specific surface area on the glycine concentration in the initial SCS mixture is presented on Fig. 7a. Specific surface area exhibits an increasing trend and reaches a maximum for 100% of glycine in the mixture. Furthermore, Scherrer's formula was employed to calculate the average crystallite size of Ni and NiO which are illustrated on Fig. 7b as a function of the specific surface area of the final products.

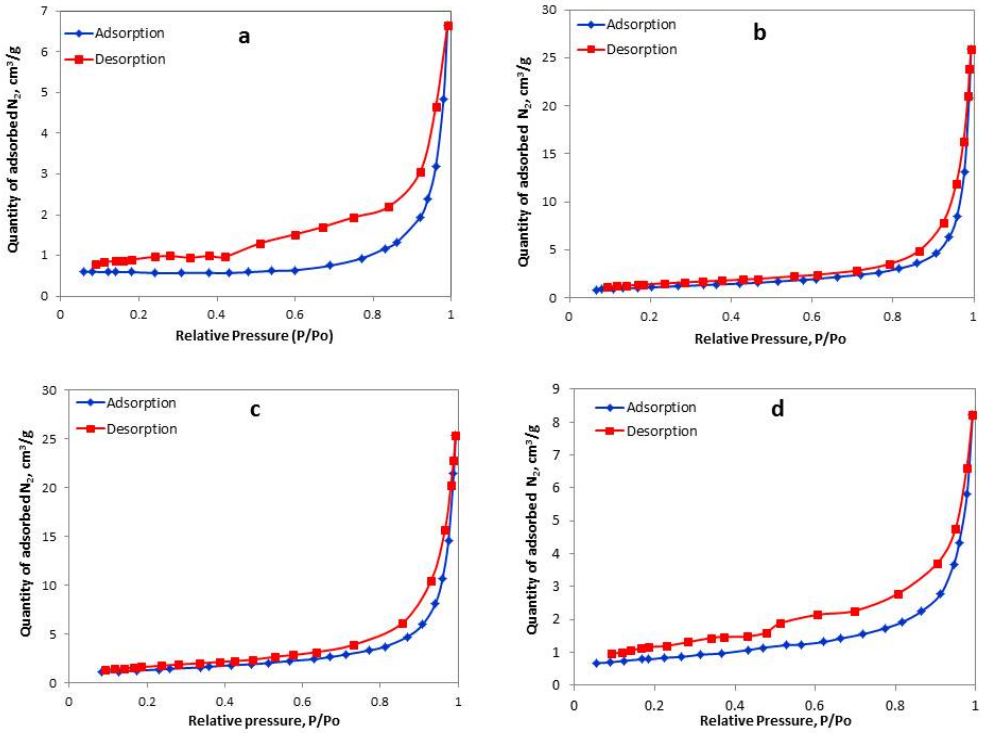

Fig. 6. Hysteresis curve of SCS materials with (a) – 50% glycine; (b) – 75% glycine; (c) – 100% glycine; (d) – 125% glycine.

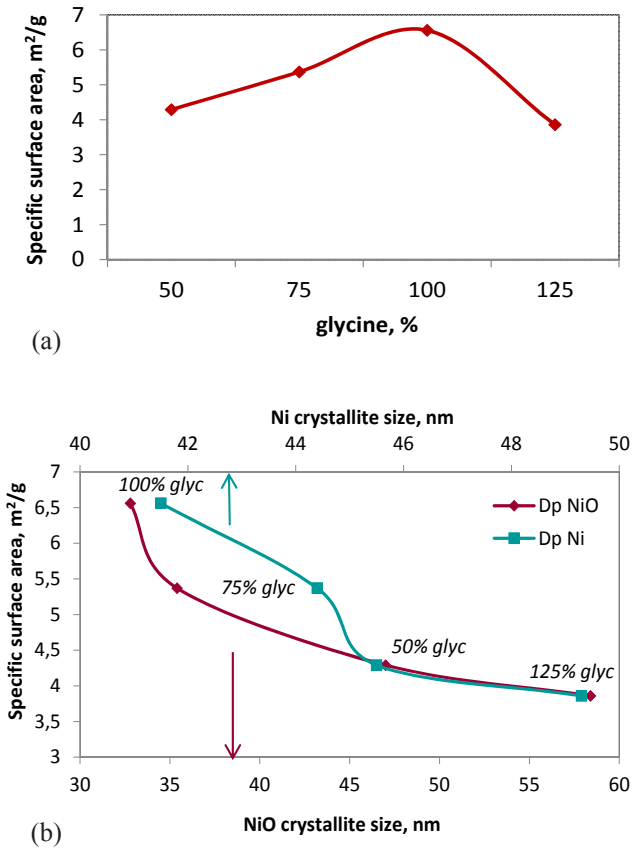

Fig. 7. (a) – Influence of glycine's concentration in SCS batch [$Ni(NO_3)_2 \cdot 6H_2O$, glycine, 100 ml water] on the final products' surface area and (b) – dependence of Ni and NiO crystallites size on SSA.

The crystallites size of both nickel and nickel oxide severely affects the materials' specific surface area. Figure 7b demonstrates that as the crystallites of nickel and nickel oxide grow, the nanomaterials' surface area reduces accordingly. Thus, when 125% of glycine was added in the initial mixture, the crystallites of nickel and nickel oxide were the largest of the measured samples, and that led to smallest specific surface area of the material. In addition it can be observed that by increasing the percentage of glycine the size of the crystallites is reduced. That can be justified by the increase of the generated gases (CO and CO_2) as the quantity of carbon increases, leading to quicker cooling rates that result in smaller crystallites. Furthermore, increasing of the crystallite size as the reducer increases can be attributed to the increase of the combustion temperature due to excessive quantity of glycine at high concentrations. That resulted in soot generation and additional heat input due to the reaction of soot combustion. Conversely, when the glycine concentration is maximized (125%) the crystallites size of nickel and nickel oxide reach their maximum as well, due to the excess of carbon concentration that causes sintering effect to take place.

Figure 8 shows the cumulative pore volume as a function of the pore diameter for the four samples prepared with different amounts of glycine in the SCS initial mixture.

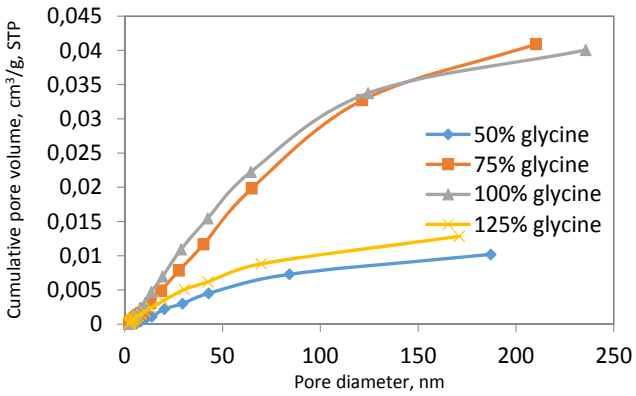

Fig. 8. Cumulative pore volume of SCS Ni catalyst with various glycine concentrations.

The pore distribution measurements shed more light on the materials microstructure. The material prepared with 50% of glycine appears to possess the minimum volume of nanopores, but smaller crystallites than the one with 125% and that justifies its slightly better SSA. As the glycine increased up to 100%, total porosity of the samples as well as the volume of nanopores was increased and that resulted in their enhanced SSA, as the sample prepared with 100% glycine had the maximum SSA. On the other hand, the sample with 125% glycine had the lowest total porosity and large crystallites of nickel and nickel oxide, and these characteristics led to its lowest SSA. The nanomaterials with smaller crystallites (obtained with 75% and 100% glycine) have higher volume of nanopores as well as increased total porosity which leads to enhanced surface area.

3. Influence of glycine concentration on slow heating mode

The SCS precursor solution contained nickel nitrate ($Ni(NO_3)_2 \cdot 6H_2O$), glycine and 75 ml distilled water. Four precursor solution were prepared by keeping the quantity of nickel nitrate constant at 9.34 g and adding four different amounts of glycine (80, 60, 50 and 40 wt% of nickel nitrate) to achieve fuel to oxidizer molar ratio (ϕ) of 2.78, 2.08, 1.74 and 1.4 for the synthesis of Ni-NiO nanopowders (ϕ = 1.0 corresponds to stoichiometry for the general SCS reaction). After preparation, the precursor solutions were placed in the furnace at room temperature and they were slowly heated up to 500 °C with an average heating rate 3 °C/min. The beaker was then placed in a pre-heated furnace at 500 °C after the end of combustion the beaker was removed from the furnace and left to cool in room temperature.

The as-synthesized phases in the SCS–derived products are displayed on the XRD patterns F in Fig. 9.

As it is illustrated on Fig. 9, nickel oxide and metallic nickel are the products of the SCS in various concentrations. This cascade of the yielded reactions during SCS is described from the following equations.

$$Ni(NO_3)_2{*}6H_2O \xrightarrow{54\ ^\circ C} Ni(NO_3)_2{*}4H_2O \xrightarrow{85.4\ ^\circ C} Ni(NO_3)_2{*}2H_2O \quad (1)$$

$$2Ni(NO_3)_2{*}6H_2O + C_2H_5NO_2 \rightarrow Ni + NiO + NO_2 + 2NO + N_2 + 2CO_2 + 29/2\ H_2O + 5/2O_2 \quad (2)$$

$$2Ni(NO_3)_2{*}6H_2O \rightarrow 2NiO + NO_2 + NO + N_2 + 6H_2O + 7/2O_2 \quad (3)$$

$$Ni(NO_3)(OH)_{2.5}{*}H_2O \rightarrow 0.5Ni_2O_3 + HNO_3 + 1.25H_2O \quad (4)\ [19]$$

$$CH_2NH_2COOH \rightarrow [CH_2COO]^- + NH_3 \quad (5)\ [19]$$

$$HNO_3 + NH_3 \rightarrow H_2O + N_2 + H_2 \quad (6)\ [19]$$

$$NH_3 \xrightarrow{Ni} H_2 + N_2 \quad (7)\ [20]$$

$$NiO + H_2 \rightarrow Ni + H_2O \quad (8)$$

$$Ni + O_2 \rightarrow NiO + 1/2O_2 \quad (9)$$

$$2CH_2NH_2COOH + 6O_2 \rightarrow 4CO_2 + 5H_2O + NO + NO_2 \quad (10)$$

$$C + O_2 \rightarrow CO_2 \quad (11)$$

$$C + NiO \rightarrow Ni + CO \quad (12)$$

$$CO + NiO \rightarrow Ni + CO_2 \quad (13)$$

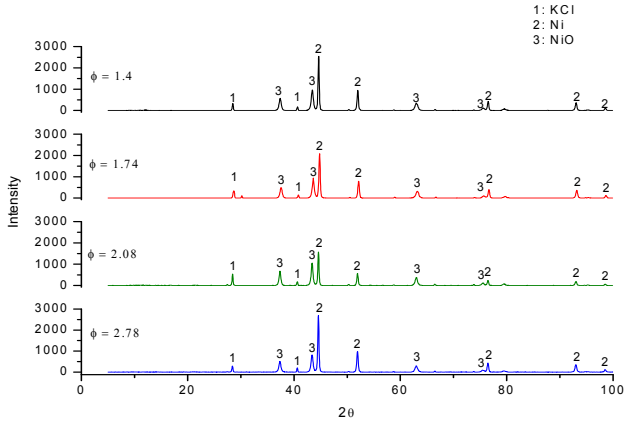

Fig. 9. Development of atomic structure of an SCS catalyst on the basis of nickel nitrate hexahydrate with glycine in various ratios.

The dependence of the relative phase composition of Ni and NiO on the ϕ ratio is presented in Fig. 10 where the variation between Ni/KCl and NiO/KCl are shown together for comparison.

Figure 10 illustrates that the variation of glycine content in the initial SCS mixture resulted in various concentrations of nickel and nickel oxide. According to the obtained data, the concentration of nickel is maximized when the concentration of the fuel is maximum as well (ϕ = 2.78), while it is minimized at ϕ = 2.08 ratio. The observed variation in the concentration of both nickel and nickel oxide is originated to the reactions' stoichiometry as well as the soot concentration in each case. The reactions' (6 and 7) stoichiometry influences the existence and the quantity of the hydrogen that it is employed for the nickel oxide reduction to produce nickel (reaction 8). Nevertheless, soot concentration, which increases by increasing the fuel content, plays a key role due to the fact that carbon is also used to reduce nickel for nickel production (reaction 7 and 8).

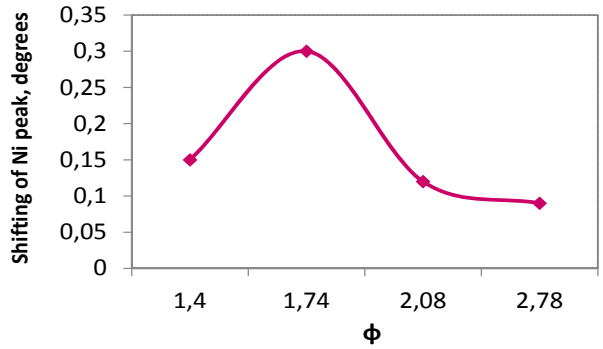

Fig. 11. The degrees of a Ni peak (2, 0, 0) shifting in the XRD spectrum as a function to ϕ ratio.

The extent of defect structure is a very important parameter for catalysts, as the defects act as active centres and influences the hydrogen adsorption on the catalytic surface in the specific case of hydrogenation reactions. On Fig. 11 below, the degrees of the nickel peak (2, 0, 0) shifting in the XRD pattern as a function to ϕ ratio is presented.

According the data obtained by XRD measurements, the peak of nickel with (h, k, l) = (2, 0, 0) was shifted in all the examined samples to the right. The catalyst prepared with ϕ = 1.74 ratio of nickel nitrate to glycine exhibited the highest shifting of the nickel peak, implying a high extent of defect structure in the crystal lattice.

The Bragg formula and Scherrer equation were employed to calculate the distance of the atomic planes and the average crystallite size of Ni and NiO which are illustrated on Figs, 12 and 13 against the ratio between nickel nitrate and glycine (ϕ).

As can be observed in Fig. 12, the increase of the fuel concentration (ϕ ratio increase) in the precursor SCS mixture solution has not a significant effect on the Ni and NiO crystal lattice spacing which reflect the crystallite nucleation conditions

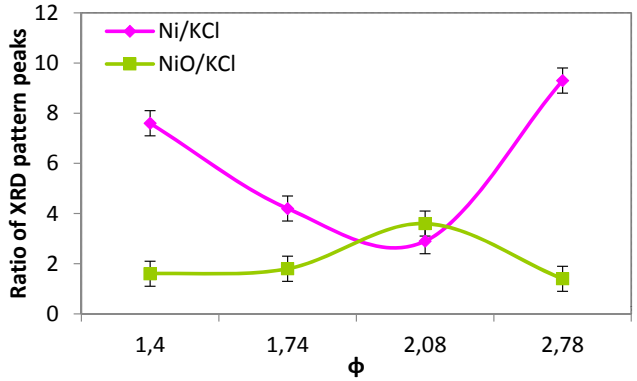

Fig. 10. Dependence of XRD peak ratio on nickel nitrate/glycine ratio in the initial SCS solution.

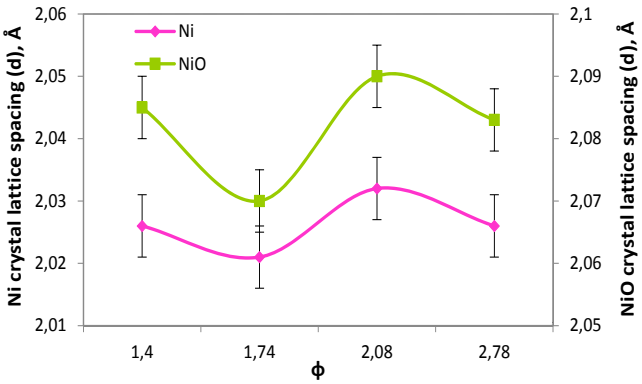

Fig. 12. Dependence of ϕ ratio on initial solution on crystal lattice spacing of the products.

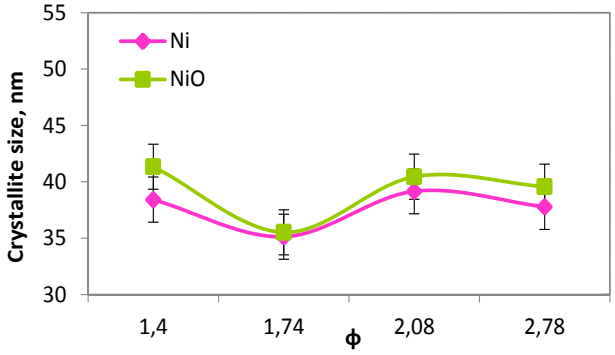

Fig. 13. Influence of φ ratio on crystallite size of the final product.

that are present in each case. The minimum value of lattice spacing in the case of ϕ = 1.74 for both Ni and NiO, is in accordance to the highest measured shifting of the XRD peaks, indicating a greater extent of the defect structure in the lattice.

Scherrer's formula revealed the crystallite size in the four catalysts for nickel and nickel oxide. There are only minor changes in the calculated crystallite size, as it is shown in Fig. 13, while the nickel crystallite size of the catalyst produced with ϕ = 1.74 is minimum, suggesting a better dispersion of the metallic phase on the nickel oxide.

Specific surface area measurements, determined by BET analysis, as a function of the ϕ ratio are presented on Fig. 14 and the specific surface area shows an increasing trend, reaching its maximum when the fuel concentration is maximized.

Generally, when the concentration of the reducer increases the carbon content increases as well, leading to an increase of the cooling due to the enhanced soot oxidation that yields during synthesis (refer to reaction 11). As a result, there is more time available for the pores to be formed, thus highest porosity is expected in the highest fuel concentration. This justifies the maximum of the specific surface area in the catalyst prepared with the highest fuel content in its initial solution.

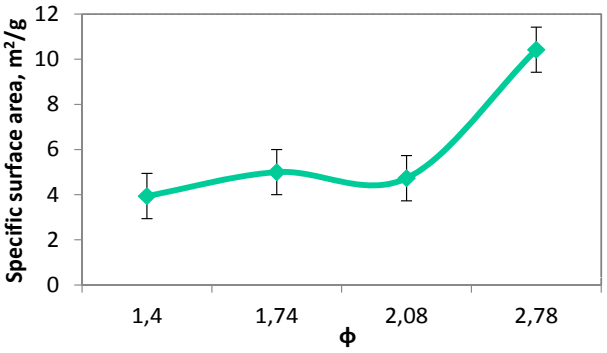

Fig. 14. Influence of ϕ ratio on the final product's specific surface area.

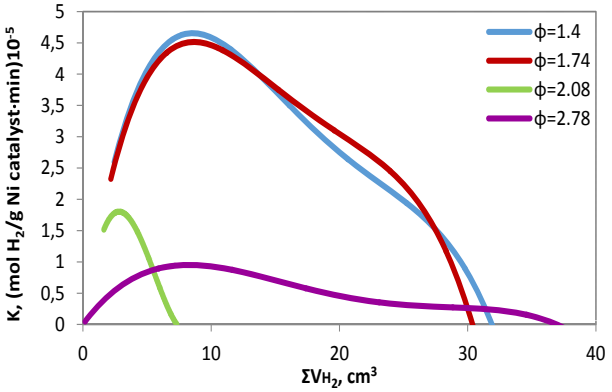

Fig. 15. Dependence of observed maleic acid hydrogenation on the SCS Ni-based catalysts on the volume of absorbed hydrogen.

The catalytic performance of the SCS-derived Ni/NiO catalysts discussed above was tested towards the hydrogenation of maleic acid in the aqueous phase. The kinetic and conversion curves that were obtained during hydrogenation are demonstrated in Figs. 15 and 16.

Figure 15 establishes the measured set of kinetics curves of the SCS catalysts with different ratio of reactants in their precursor solution. The catalysts prepared with relatively low ϕ ratio appear to be most active, while the catalysts made with higher ϕ exhibited very low activity (ϕ = 2.78) or were almost inactive (ϕ = 2.08). Conversion curves of the catalysts are displayed on Fig. 16.

The degree of conversion of maleic acid into succinic acid is very low (17.2%) for the catalysts with ϕ = 2.08, whereas the other three catalysts exhibit better catalytic activity, with the catalyst produced with ϕ = 2.78 showing the highest conversion rates. These results correlate well with the catalysts' kinetic curves (Fig. 15). Notably, the catalyst prepared with ϕ = 2.78 exhibited higher percentage of

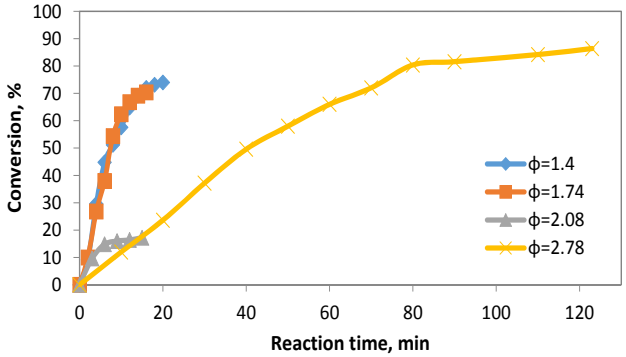

Fig. 16. The dependence of maleic acid conversion on the SCS catalysts calculated from the quantity of absorbed hydrogen.

conversion than those made with ϕ = 1.4 and ϕ = 1.74, even though the latter showed significantly higher velocity during hydrogenation. Catalysts with ϕ = 1.40 and ϕ = 1.74 exhibited high velocity towards the hydrogenation of maleic acid that can be attributed to the high concentration of Ni and in high defect structure, accordingly. Furthermore, neither of the catalysts tested achieved 100% conversion, suggesting that the produced succinic acid was strongly adsorbed on the catalysts surface leaving no available space for new hydrogen molecule to adsorb and react with maleic acid.

The extent by which the surface was coated with hydrogen is a critical parameter that determines catalytic activity, as all catalytic reactions take place on the catalyst surface. In the Fig. 17 that is shown below, the percentage of hydrogen surface coating on catalysts in correlation with their activity in liquid-phase hydrogenation is illustrated as a function to the ϕ ratio.

There is a correlation between the percentage of the hydrogen surface coating and the catalysts measured activity toward the maleic acid's hydrogenation. The catalysts prepared with a relatively low ϕ ratio exhibited the maximum velocity over the reaction, while the catalyst made of ϕ = 2.08 shown the lowest velocity. The percentage of the hydrogen surface coating is affected by various parameters. Some of the most important ones are the concentration of nickel and the extent of the defect structure in the catalyst's volume. Specifically, the catalyst with ϕ = 1.4 ratio of reactants has the maximum percentage of hydrogen coating on its surface due to its high nickel content (Fig. 10) and as a result was the most active. By increasing ϕ to 1.74 the percentage of hydrogen decreases, due to its lower nickel content. Noticeably, the catalyst's activity is not severely influenced because of its highest extent of defect structure, as presented on Fig. 11 and its highest dispersion of nickel on nickel oxide (suggested by Fig. 13). Moreover, when the fuel content in the initial mixture maximizes (ϕ = 2.78), the additional heating provided by the soot oxidation leads to enhancement of the sintering process resulting in the elimination of defects in the metal crystallites, which are responsible for the catalytic activity [21]. This conclusion is consistent to the measured shifting of the nickel's peak in the XRD spectrum (Fig. 11) and explains the minimum percentage of hydrogen coating on the catalyst's surface, despite its maximum nickel concentration. Finally, the catalyst prepared with ϕ = 2.08 was almost inactive due to its lowest nickel content (Fig. 10) with small dispersion on the nickel oxide (Fig. 13) and its relatively low percentage of hydrogen surface coating.

Nevertheless, there is a sufficing correspondence between the catalysts' conversion of maleic acid to succinic acid during hydrogenation and the calculated nickel content in their mass (Fig. 18). The decrease of nickel content from ϕ = 1.4 to ϕ = 1.74 is not accompanied with a decrease in the catalysts conversion as it has the highest dispersion of the metallic phase on nickel oxide and the highest shifting of nickel's XRD peak that suggest highest extent of defect structure (Fig. 11). Interestingly, in case of ϕ = 2.78, the as-synthesized catalyst exhibited highest conversion, despite its low velocity during hydrogenation, originating to its maximum nickel content and specific surface area (Fig. 14).

The same series of experiments only with different heating mode were performed and published by Xanthopoulou et al. [22]. In comparison to those experiments, it appears that when the slow heating mode is applied, the nickel content in the final catalytic nanomaterials is reduced. Moreover, the nickel crystallites is also reduced and ranges

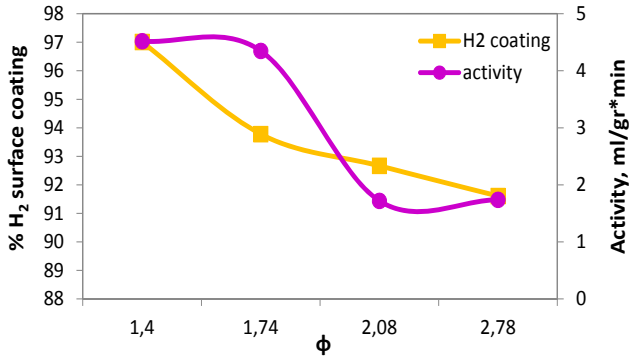

Fig. 17. SCS catalysts' hydrogen surface coating and activity as a function of the reactants ratio (ϕ).

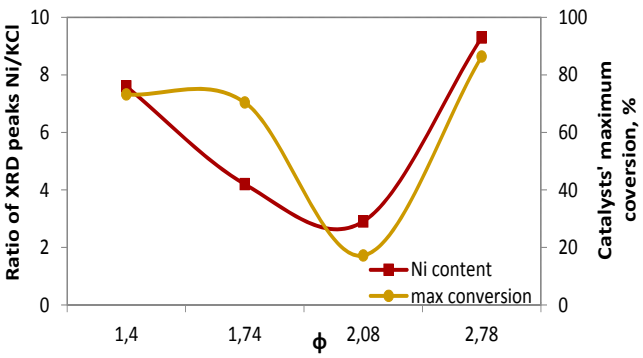

Fig. 18. Dependence of SCS catalysts' nickel concentration and conversion from the reactants' ratio (ϕ).

between 35–40 nm, while in the other mode is ranges between 40–49 nm. That can be explained as in the case of slow heating, a big part of the nickel nitrate is already decomposed in nickel oxide, before the time the mixture reaches its ignition point. As a result, there is less quantity of nitrate available to react and participate in the SCS, leading to lees nickel concentration in the final products. Moreover, the lessened quantity of nitrate that participates in the SCS reduces the heat that is emitted from the exothermic reaction. Consequently, there is less sintering process taking place that justifies the reduction in the size of nickel crystallites.

4. Influence of the time in furnace after SCS is completed

The precursor SCS mixture consisted of 66.7% nickel nitrate hexahydrate [$Ni(NO_3)_2 \cdot 6H_2O$] as oxidizer, 33.3% glycine as reducer and 75 ml of distilled water. The total solid mass of the initial mixture was 14 g. Each solution was pre-heated on a hot plate with mild magnetic stirring until 70 °C and it was then placed in a pre-heated furnace at 500 °C for the SCS to take place. After the completion of the SCS cascade of reactions the beaker was left in the furnace for various time periods (0, 2, 7, 10 min) and four materials were derived.

The as-produced materials were characterized by XRD analysis and the resulting patterns are exhibited on Fig. 19.

The obtained XRD patterns demonstrate the resulted nickel and nickel oxide phases in the final materials. Their different concentrations in the as-burnt products are demonstrated on the semi-quantitative analysis, using KCl as an internal standard (Fig. 20).

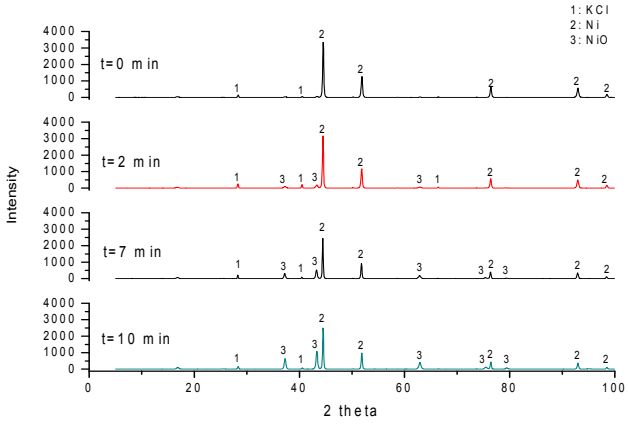

Fig. 19. XRD patterns from the SCS – derived materials on the basis of initial mixture 66.7% $Ni(NO_3)_2 \cdot 6H_2O$ and 33.3% glycine with various periods of time remaining in the furnace after SCS was completed.

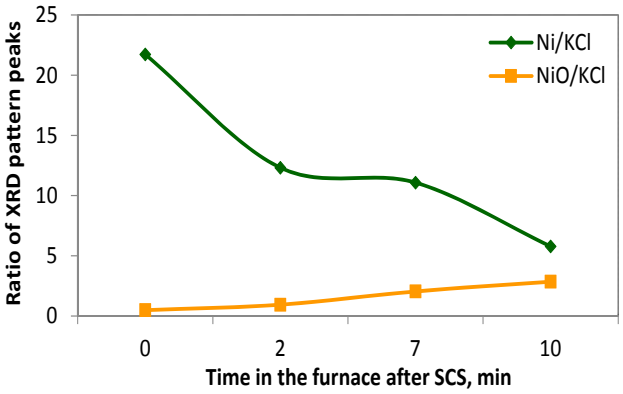

Fig. 20. Influence of time in furnace after SCS on the Ni and NiO relative phase concentration in the resulting materials.

Figure 20 shows the concentration of nickel and nickel oxide in each sample that remained in the furnace after the SCS ended. Increasing the time that the sample remained in the furnace the concentration of nickel is reduced while the nickel oxide content increases. The remaining of the samples in such a high temperature supplies more time for the oxidation of nickel to take place due to the furnace's oxidative atmosphere. In conclusion, immediate cooling is suggested in order to achieve maximum nickel content in the produced material. This can also be certified by the obtained time resolving XRD analysis pattern, which is presented on Fig. 21.

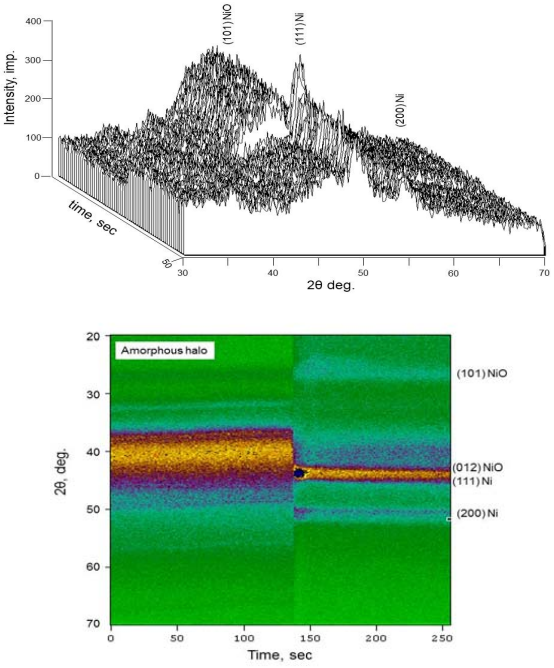

Fig. 21. Results of time-resolved X-ray diffraction analysis in a SCS gel.

In Fig. 21 a sequence of 50 XRD traces obtained by time-resolved X-ray diffraction (TRXRD) studies(measured each second) depicts the phase formation process as solution combustion synthesis takes place. The spectra are presented in both 2D of 2θ versus time as well as in 3D of 2θ versus intensity versus time. The precursor nitrate-glycine mixture provides a diffraction pattern with wide amorphous halo suggesting that the phases are not crystallized. During the ignition of combustion, nickel lines (111) and (200) appear first and within a few seconds their intensity increases. Thereafter, a reduction of their amplitude and the NiO lines (101) and (012) that appear at the same time is exhibited. This indicates that after the formation of nickel, its concentration decreases with time with the simultaneous increase of NiO concentration.

The influence of the time period that the samples remained in the furnace after SCS completion on the crystallites size of nickel and nickel oxide is presented on Fig. 22.

According to the calculated results from Scherrer's formula, by increasing the time in the furnace, the crystallites of both nickel and nickel oxide are increasing as well. The sintering process that takes place when the samples are not immediately removed from the furnace results in the observed growth of the crystallites for both phases. As a conclusion, smaller crystallites are obtained when the beaker is removed from the furnace by the time the SCS reactions are finished.

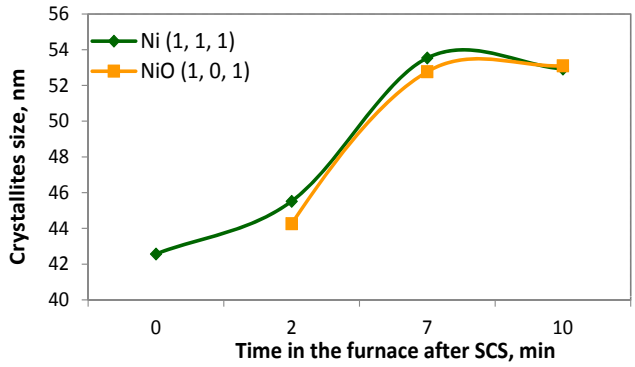

Fig. 22. Influence of the timed remained in the furnace after the SCS completion on crystallites size of Ni and NiO.

5. Conclusions

1. The increase of the oxidizer quantity affects only the generated heat from the combustion, thus the cooling time is prolonged. On the other hand, there is a specific time for the formation of nickel as well as for its oxidation. Consequently, the maximum in the nickel content can be attributed to the initial increase of time for nickel formation, while after exceeding critical amount there is enough time for nickel oxidation as well.

2. At the excess(over stoichiometric concentration) of glycine (125%), the carbon originated from glycine is employed to the soot oxidation reaction lead to rising combustion temperature and resulted in reduction of nickel content in the SCS product. In this case, carbon is the major element that reduces nickel oxide for the production of nickel, and not hydrogen as it was in the case of 50% glycine.

3. Concentration of reducer affects porous structure of nanomaterial and the form of pores. Regarding the shape of the hysteresis loops, the adsorption/desorption isotherms of samples with 50 and 125% glycine correspond to type B, suggesting the existence of large number of cylindrical and slit-shape pores with all open sides. On the other hand, the type of loop in samples with 75 and 100% glycine are type C indicating that the pores have a predominately wedge shape. The pore shape affects the adsorption – desorption process during catalysis influencing the exhibited activity of catalysts.

4. It was determined, that if crystallites of nickel and nickel oxide grow, the nanomaterials' surface area reduces accordingly. By increasing the percentage of glycine (from 50 to 100%) the size of the crystallites is reduced. That can be justified by the increase of the generated gases (CO and CO_2) as the quantity of carbon increases, leading to quicker cooling rates that result in smaller crystallites. Furthermore, increasing + the crystallite size as the reducer increases can be attributed to the increase of the combustion temperature due to excessive quantity of glycine at high concentrations which lead to sintering process. Nanomaterials with smaller crystallites (75% and 100% glycine) have higher volume of nanopores and higher porosity which lead to enhanced specific surface area.

5. The fuel concentration affects the catalytic activity as catalysts with ϕ =1.40 and ϕ = 1.74 exhibited the highest velocity towards the hydrogenation of maleic acid due to its high concentration of Ni and its high defect structure, accordingly. Moreover, their enhanced catalytic behavior can be originated to their high percentage of hydrogen coating on the surface.

6. It appears that when the slow heating mode is applied, the nickel content in the final catalytic nanomaterials is reduced. Moreover, the

nickel crystallites is also reduced and ranges between 35–40 nm, while in the other mode is ranges between 40–49 nm. That can be explained as in the case of slow heating, a big part of the nickel nitrate is already decomposed in nickel oxide, before the time the mixture reaches its ignition point. As a result, there is less quantity of nitrate available to react and participate in the SCS, leading to less nickel concentration in the final products. Moreover, the lessened quantity of nitrate that participates in the SCS reduces the heat that is emitted from the exothermic reaction. Consequently, there is less sintering process taking place that justifies the reduction in the size of nickel crystallites.

7. TRXRD measurements indicate that after the formation of nickel, its concentration starts to decrease with time, while the concentration of NiO increases. That explains the reason that the time in the furnace after SCS finalized leads to increasing of NiO/Ni phase ratio. By increasing the time in the furnace, the crystallites of both nickel and nickel oxide are increasing as well due to the sintering process that takes place.

Acknowledgements

We would like to thank Dr. D. Kovalev from the Institute of Structural Macrokinetics and Materials Science in Russia for TRXRD analysis.

We would also like to thank Dr. N. Boukos from the Institute of Nanoscience and Nanotechnology in NCSR “Demokritos” Greece for TEM captions and analysis.

References

[1]. A.S. Mukasyan, P. Epstein, P. Dinka, *Proc. Combust. Inst.* 31(2007) 1789–1795. DOI: 10.1016/j.proci.2006.07.052

[2]. K.C. Patil, S.T. Aruna, S. Ekambaram, *Curr. Opin. Solid State Mater. Sci.* 2 (1997) 158–165. DOI: 1359-0286-002-00158

[3]. F. Li, J. Ran, M. Jaroniec, S.Z. Qiao, *Nanoscale* 7 (2015) 17590–17610. DOI: 10.1039/C5NR05299H

[4]. S.L. González-Cortés, F.E. Imbert, *Appl. Catal. A* 452 (2013) 117–131. DOI: 10.1016/j.apcata.2012.11.024

[5]. G. Xanthopoulou, O. Thoda, E.D. Metaxa, G. Vekinis, A. Chroneos, *J. Catal.* 348 (2017) 9–21. DOI: 10.1016/j.jcat.2016.12.002

[6]. S.T. Aruna, A.S. Mukasyan, *Curr. Opin. Solid State Mater. Sci.* 12 (2008) 44–50. DOI: 10.1016/j.cossms.2008.12.002

[7]. O. Thoda, G. Xanthopoulou, G. Vekinis, A. Chroneos, *Adv. Eng. Mater.* 20 (2018) 1800047. DOI: 10.1002/adem.201800047

[8]. A. Varma, A.S. Mukasyan, A.S. Rogachev, K. V. Manukyan, *Chem. Rev.* 116 (2016) 14493–14586. DOI: 10.1021/acs.chemrev.6b00279

[9]. P. Ravindranathanan, K.C. Patil, *J. Mater. Sci. Lett.* 5 (1986) 221–222. DOI: 10.1007/BF01672056

[10]. K. Deshpande, A.S. Mukasyan, A. Varma, *Chem. Mater.* 16 (2004) 4896-4904. DOI: 10.1021/cm040061m

[11]. S. Challagulla, S. Roy, *J. Mater. Res.* 32 (2017) 2764–2772. DOI: 10.1557/jmr.2017.244

[12]. A.B. Salunkhe, V.M. Khot, M.R. Phadatare, S.H. Pawar, *J. Alloys Comp.* 514 (2012) 91–96. DOI: 10.1016/j.jallcom.2011.10.094

[13]. K.B. Podbolotov, A.A. Khort, A.B. Tarasov, G.V. Trusov, S.I. Roslyakov, A.S. Mukasyan, *Combust. Sci. Technol.* 189 (2017) 1878–1890. DOI: 10.1080/00102202.2017.1334646

[14]. B. Pourgolmohammad, S.M. Masoudpanah, M.R. Aboutalebi, *J. Magn. Magn. Mater.* 424 (2017) 352–358. DOI: 10.1016/j.jmmm.2016.10.073

[15]. O. Thoda, G. Xanthopoulou, G. Vekinis, A. Chroneos, *Catal. Lett.* 148 (2018) 764–778. DOI: 10.1007/s10562-017-2279-y

[16]. H. Ajamein, M. Haghighi, *Energy Convers. Manag.* 118 (2015) 231–242. DOI: 10.1016/j.enconman.2016.04.002

[17]. J.H De Boer. The structure and properties of porous materials, London: Butterworth. In: Proceedings of the tenth symposium of the Colston Research Society held in the University of Bristol, London: Butterworths, 1958, pp. 68–94.

[18]. B. Nie, X. Liu, L. Yang, J. Meng, X. Li, *Fuel* 158 (2015) 908–917. DOI: 10.1016/j.fuel.2015.06.050

[19]. A. Kumar, E.E. Wolf, A.S. Mukasyan, *AlChe Journal* 87(2011) 2207–2214. DOI: 10.1002/aic.12416

[20]. A.M.M. Santos, W.L. Vasconcelos, *Mater. Res.* 2 (1999) 201–204. DOI: 10.1590/S1516-14391999000300015

[21]. J.L. Carter, J.A. Cusumano, J.H. Sinfelt, *J. Phys. Chem.* 70 (1966) 2257–2263. DOI: 10.1021/j100879a029

[22]. G. Xanthopoulou, O. Thoda, S. Roslyakov, A. Steinman, E. Levashov, D. Kovalev, G. Vekinis, A. Sytschev, A. Chroneos, *J. Catal.* 364 (2018) 112–124. DOI: 10.1016/j.jcat.2018.04.003